Strengthening of Reinforced Concrete Slabs using Macro and Micro Synthetic Fibers

S. M. Iqbal S. Zainal[1], Farzad Hejazi[2,*], Ala M. A. Mafaileh[3]

[1] *Faculty of Engineering, Universiti Malaysia Sabah, Kota Kinabalu 88400, Sabah, Malaysia*
[2] *Faculty of Environment and Technology, University of The West of England, Bristol BS16 1QY, United Kingdom*
[3] *Department of Civil Engineering, Universiti Putra Malaysia, Serdang 43400, Selangor, Malaysia*
[*]Correspondence: farzad.hejazi@uwe.ac.uk

Abstract
Concrete is brittle and prone to cracking, especially under tensile forces. The gradual development and propagation of cracks would subsequently lead to brittle failure. The use of fibers is effective in restricting the propagation of cracks and improving the failure mode of cement composites. This study attempts to enhance the performance of Reinforced Concrete (RC) slabs under a four-point bending test by embedding synthetic fibers with distinct parameters. In the preliminary stage, experimental uniaxial tests were conducted in compression and tension to observe the stress-strain behavior of the developed Hybrid Fiber Reinforced Concrete (HyFRC). The obtained data are then used as input in Finite Element (FE) modeling for numerical analyses. In the primary stage, the numerical results were verified from the experimental data with respect to cracking behavior, ultimate load capacity, corresponding mid-span deflection, and steel reinforcement strain output. Based on the results, the HyFRC slabs exhibited positive improvements in terms of load-carrying capability by reducing stress in the concrete and rebars. The HyFRC slabs also experienced lower deflections with improved crack resistance and high flexural stiffness than the control slab. Additionally, the developed FE models presented a low margin of error compared to the experimental data for all assessed criteria.

Keywords: hybrid fiber reinforced concrete, constitutive modeling, synthetic fibers, reinforced concrete slab, flexural strength, uniaxial test.

1. Background

Fiber Reinforced Concrete (FRC) was defined by the ACI 116R, Cement and Concrete Terminology as concrete containing dispersed randomly oriented fibers. These fibers provide 3-dimensional reinforcement in cementitious composites, which is advantageous in limiting the inducement of large loads to primary steel reinforcements from all directions. Reinforcing concrete with high strength and short fibrous material has long been used and can be dated to approximately 3,500 years ago. Ancient civilizations used thatches to reinforce brittle sun-dried bricks, straw fibers to enhance baked-clay mud huts, animal hairs for masonry mortars, and many more to improve the mechanical properties of construction materials at that time. Several investigations have already shown FRC improving the performance of conventional concrete in tensile strength, compressive strength, elastic modulus, crack resistance, crack control, durability, fatigue life, resistance to impact and abrasion, shrinkage, expansion, thermal characteristics, and fire resistance [1]–[5].

FRC can be classified into four categories – Type I (steel), Type II (glass), Type III (synthetic), and type IV (natural) [6]. Steel fibers have been popular since the 1970s because of the substantial improvement it imparts on concrete. However, recent advancement in petrochemical and textile industries has led to the widespread use of synthetic materials because of their fast manufacturing process, economical price, new types of organic fibers, and versatile applications [7], [8]. Several companies have begun manufacturing macrosynthetic fibers, a synthetic fiber on a macro-sized scale, which has been claimed to replace secondary steel reinforcements [9], [10]. In addition, the application of FRC in different beam-column joint have been studied by several researchers, and the results showed improvement in the beam-column structural ductility [11]–[14]. The fiber application in cement matrix harbors great potential by the possible reduction of steel reinforcements in the beam-column joint regions while providing a more straightforward connection design without the ductile detailing complications that commonly ensue.

The use of single-fiber in FRC also limits the fiber-bridging capabilities because they are bounded by crack zones and volume fraction limitations. Cracking is a multiscale and gradual process; microcracks coalesce into macrocracks, propagating at a stable rate until instability occurs and fractures the cementitious composites. The use of only one type of fibers implies that the fiber would only be able to reinforce one level of crack and within its cracking-strain limit [15]–[18]. Hence, high-volume fractions of fiber are typically designed to overcome the strain limit, but then this causes problems such as workability complications during concrete casting [19]. In general, micro and macro synthetic fibers are fibers manufactured from synthetic materials with diameters smaller than 0.3mm and larger than 0.3mm, respectively. By hybridizing micro and macro synthetics from two or more different materials in a cement matrix, the Hybrid Fiber Reinforced Concrete (HyFRC) can reinforce a higher range of crack levels, reduce applied damage and achieve equal or greater performance capability than using single-FRC. HyFRC combinations were also more effective than traditional FRC in bridging micro-crack, resulting in strain-hardening of concrete and improving the post-cracking mode of failure [20]–[23].

Fibers are usually hybridized between a primary load-bearing fiber and a secondary fiber. Steel fibers are widely popular in being considered as the load-bearing fiber in any combination mix because of their high strength, stiffness, ductility, and large macro-size compared to the other types of fiber [1], [24]–[26]. However, recent developments in producing macrosynthetic fibers might break the over-dependency on steel fibers as the primary choice for load-bearing fibers. Macro-sized synthetic fibers are more advantageous to be used because it is more economical than steel fibers and has been reported to achieve similar reinforcing capabilities [3], [27], produce a significantly lower carbon footprint [28], [29], and non-corrosive in nature compared to steel, which was known to deteriorate in performance over time. Furthermore, the use of steel fibers higher than 2% in concrete also led to fiber segregation and air entrapment, affecting the fibers' tensile and flexural stress-resisting capabilities [30]. There is currently limited literature on the strengthening of concrete slabs with different synthetic fiber hybridization, which warrants further research.

In summary, it can be deduced that the most advantageous type of fibers to be used in RC structures are synthetic fibers due to their resultant ductility improvements. Hybridizing multiple different types of synthetic fibers would improve the crack fiber-bridging effect in cementitious composites, allowing them to absorb more energy than single-fibers. Therefore, it can be hypothesized that the developed HyFRC in this research would strengthen and improve the performance of RC slabs. Numerical models would then be developed using commercial FE software and verified against the experimental results for future applications using the developed novel materials.

2. Mix Design of Hybrid Fiber Reinforced Concrete

In this investigation, 5 HyFRC mix designs have been developed. Each of the synthetic fibers has distinct characteristics, as shown in Table 1. The PP macrosynthetic fibers are chosen as the load-bearing fiber in the hybridization with a controlled volume fraction of 0.6% from the weight of cement. Varying lengths of PP fibers were combined (38 and 54 mm) to improve the HyFRC yield strength [31] and post-cracking behavior [32]. P1, P2, P3, and N fibers are micro-sized fibers added in the mix proportions to evoke the concrete multi-cracking phenomenon and prevent centralized single-crack propagations [33], which have been known to result in rapid brittle cracks. All the synthetic fibers used in the mix design are shown in Figure 1.

Table 1: Properties of Fibers

Fiber Name	PP	P1	P2	P3	N
Material	Polypropylene, Polyethylene	Polypropylene	Polypropylene	Polypropylene	Nylon
Fiber Type	Macro	Micro	Micro	Micro	Micro
Fiber Form	Fibrillated twisted bundle	Collated fibrillated twisted bundle	Collated fibrillated	Collated fibrillated	Monofilament
Tensile Strength (MPa)	570-660	570-660	570-660	570-660	966
Interfacial Bond	Strong	Strongest	Strong	Moderate	Weak
Specific Gravity	0.91	0.91	0.91	0.91	1.14
Density (kg/m3)	910	910	910	910	1150
Length (mm)	38, 54	54	38	19	19
Color	Gray	Tan	Gray	White	White
Acid/alkali resistance	Excellent	Excellent	Excellent	Excellent	Good

The bonding power in the fiber properties refers to the interfacial bond between the fibers and cement matrix during fiber pull-out, while the tensile strengths correspond to the single-fiber strength of respective synthetic fibers. PP and P1 fibers have a twisted bundle form which enhances pegging of the fibers in concrete during failure. The type II Ordinary Portland cement used in this study satisfies the chemical and physical requirements of the ASTM C150 standard [34].

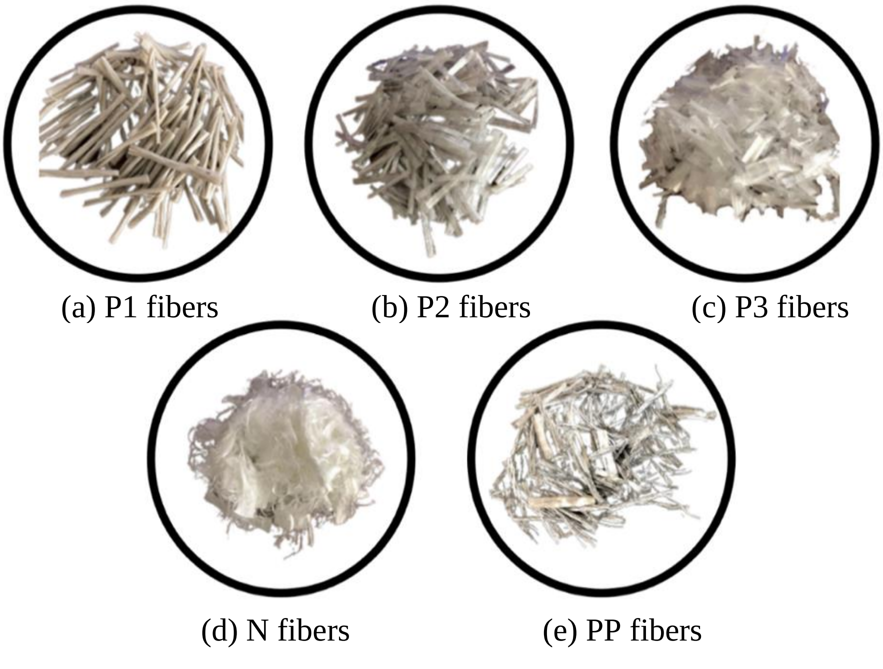

Figure 1: Synthetic fibers used in this study

An aqueous solution of modified polycarboxylate superplasticizer was added to the HyFRC mixture to improve the workability issues associated with Fiber Reinforced Concrete as well as to enhance the mechanical properties. The superplasticizer complies with the ASTM C494 standard [35] under the Type F classification. Each of the detailed HyFRC mix proportions is shown in Table 2. The ratio for 10mm and 20mm coarse aggerates was fixed at 1:2.

Table 2: Mix Design

Materials	Unit	Control	HyFRC 1	HyFRC 2	HyFRC 3	HyFRC 4	HyFRC 5
Cement	kg/m^3	409.00	409.00	409.00	409.00	409.00	409.00
Fine aggregate	kg/m^3	836.00	836.00	836.00	836.00	836.00	836.00
Coarse aggregate	kg/m^3	906.00	906.00	906.00	906.00	906.00	906.00
PP (38mm)	Volume fraction, V_f (%)	-	0.60	0.60	0.60	0.60	0.60
PP (54 mm)	Volume fraction, V_f (%)	-	0.60	0.60	0.60	0.60	0.60
P1	Volume fraction, V_f (%)	-	-	0.30	-	-	-
P2	Volume fraction, V_f (%)	-	-	-	0.30	-	-
P3	Volume fraction, V_f (%)	-	-	-	-	0.30	-
N	Volume fraction, V_f (%)	-	-	-	-	-	0.30
Superplasticizer	%(volume)	-	0.6	0.6	0.8	0.7	0.8
Total water	ℓ/m^3	225.00	225.00	225.00	225.00	225.00	225.00
w/c ratio	-	0.55	0.55	0.55	0.55	0.55	0.55

An admixture parametric study was conducted to ensure consistent dispersion of fibers in cement matrix as well as to improve the fresh and hardened performance of the HyFRC. Incremental superplasticizers were added to the mix designs to evaluate the corresponding slump and compressive strength results. A total of 3 cubes with 100x100x100mm dimensions were crushed for every increase in superplasticizer dosage at 28-days moist-curing age. The slump test results are shown in Figure 2, while the corresponding 28-days compressive strengths are tabulated in Table 4. An optimal superplasticizer dosage was chosen as an attempt to balance between workability and corresponding hardened strength. It can be concluded from the results that the optimal superplasticizer dosage is 0.6% for HyFRC 1, HyFRC 4, and 0.8% for HyFRC 2, HyFRC 3, HyFRC 5.

3. Methodology

3.1 Uniaxial Tests

The uniaxial compressive test was conducted to observe the elastic and plastic behavior of the developed HyFRC in compression. The test setup adheres to the ASTM C469 [36] standard with improvisations to measure the post-cracking degradation of concrete [37]. In order to improve the deflection measurement during the elastic cracking instability, two 100 mm LVDTs were positioned parallel to the crosshead movement of the UTM plate by magnetic clamp holders to record the plastic strain of the HyFRC cylinders during post-cracking, as shown in Figure 3a. Additionally, a 2000 kN Universal Testing Machine (UTM) with a loading rate of 0.02 mm/s was used to test twelve 15 x 300 mm cylindrical specimens under compression. A double-loop circular jig was securely fixed on the cylinder specimens to hold two 50 mm Linear Variable Displacement Transducers (LVDT) for elastic strain measurements.

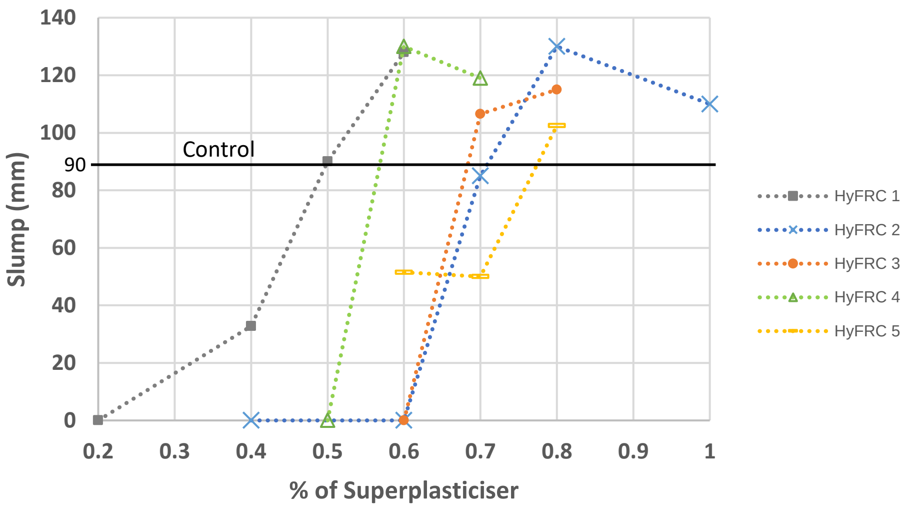

Figure 2: Admixture parametric study.

Table 3: Corresponding slump and 28-days Compressive Strength (CS).

Superplasticizer (%)	HyFRC 1		HyFRC 2		HyFRC 3		HyFRC 4		HyFRC 5	
	Slump (mm)	CS (MPa)	Slump (mm)	CS (MPa)	Slump (mm)	CS (MPa)	Slump (mm)	CS (MPa)	Slump (mm)	CS (MPa)
0.2	0 ₠	43.97	-	-	-	-	-	-	-	-
0.3	-	-	-	-	-	-	-	-	-	-
0.4	132.5	31.87	0 ₠	-	-	-	-	-	-	-
0.5	90	40.67	-	-	-	-	0 ₠	48.52	-	-
0.6	128	41.43	0 ₠	45.69	0 ₠	46.51	130	40.44	57.5	48.21
0.7	-	-	85	25.93	106.5	47.01	119	49.15	50	49.66
0.8	-	-	130	24.86	115	49.41	-	-	102.5	41.89
0.9	-	-	-	-	-	-	-	-	-	-
1.0	-	-	110 §	26.47	-	-	-	-	-	-

₠ - aggregate segregation observed
§ - concrete bleeding observed

(a) Compressive Test (b) Tensile Test

Figure 3: Uniaxial Tests for Stress-Strain HyFRC Observation

The assessment of tensile behavior for the developed HyFRC was based on the ASTM E8 standard [38], with modifications conducted on the setup to accommodate the HyFRC sample requirement [37]. In the material sample modification, the dog-bone HyFRC specimens were cast with a 10 mm notch sawed on the mid-span to define the failure plane. Additionally, the gauge section was designed to be thicker than the longest fiber used (54 mm) to avoid the fiber balling effect as well as to enable consistent fiber distribution in the cement composite. In the setup modification, two 50mm LVDTs were clamped near the mid-section of the dog-bone specimen, as shown in Figure 3(b), to measure the displacement along the length of the cross-section. A total of twelve dog-bone specimens were cast with a length of 500 mm and a cross-section of 80 x 120 mm, which narrows to an 80 x 80 mm narrow mid-gauge section.

3.2 Finite Element Modeling

One of the challenges faced in testing new materials for structural applications is the unavailability of these materials in the commercial FEA materials library for numerical analyses. This research intends to record the developed HyFRC stress-strain behavior and use it as a preliminary record in the FE materials library. In this manner, more cost-effective testing can be established as high-performing HyFRC specimens can be tested for moderate-scale experimental validations. Furthermore, it is more viable to observe the preliminary validations and improve the fiber characteristics before a full-scale experimental HyFRC slab can be conducted.

Five HyFRC and one control slab models were created in ABAQUS Computer Aided Engineering (CAE) software. The stress-strain data obtained from the uniaxial testing is incorporated into the Concrete Damaged Plasticity (CDP) section, which numerically governs

the corresponding behavior of the slabs under cyclic loading. The density and Poisson's ratio of the modeled concrete were defined as 2400 kg/m^3 and 0.2, correspondingly. Additionally, the four input parameters that were required to describe the CDP, such as dilation angle (ψ), plastic flow potential eccentricity (ϵ), the ratio of biaxial to uniaxial compressive strengths (σ_b/σ_o), and the shape factor (Kc) were all set to default values, of 31°, 0.1, 1.16, and 0.67, respectively.
For this study, 800 x 600 mm HyFRC slab with 80 mm thickness and C30 concrete grade were modeled. Details of the developed numerical models are shown in Figure 4, where 7 bars with 10 mm diameter were used as main reinforcement at 95 mm c/c spacing, and 4 bars of 8 mm diameter were used as distribution reinforcement at 125 mm c/c spacing.

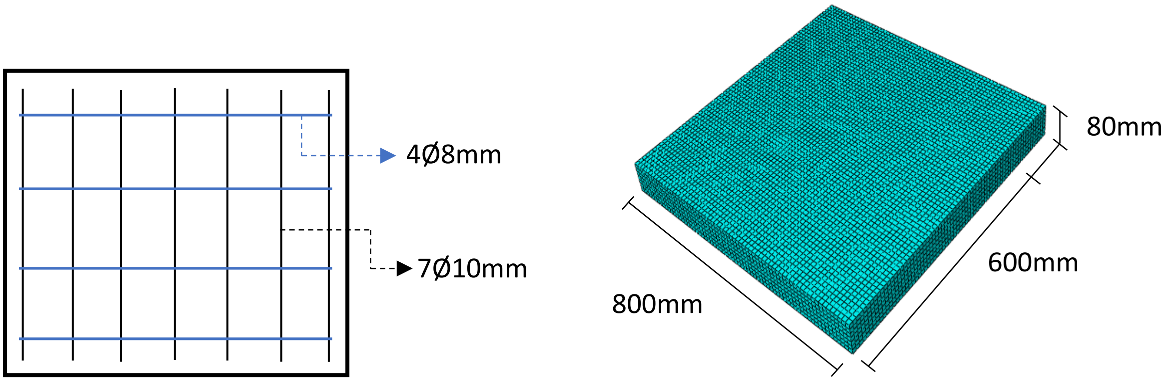

(a) Embedded rebars (b) Model dimension

Figure 4: HyFRC numerical models.

The slabs were modeled with the C3D8R brick element with 3 degrees of freedom at each node to achieve a uniform stress distribution. T3D2 elements with 3 translational degrees of freedom were selected to model the reinforcing steel bars. A 100 mm global mesh size was also selected based on the conducted convergence mesh study. The load was introduced at the center of the top slab section with the corner edges of the slab bottom section fixed to prevent any translational and rotational movements, as shown in the boundary conditions in Figure 5.

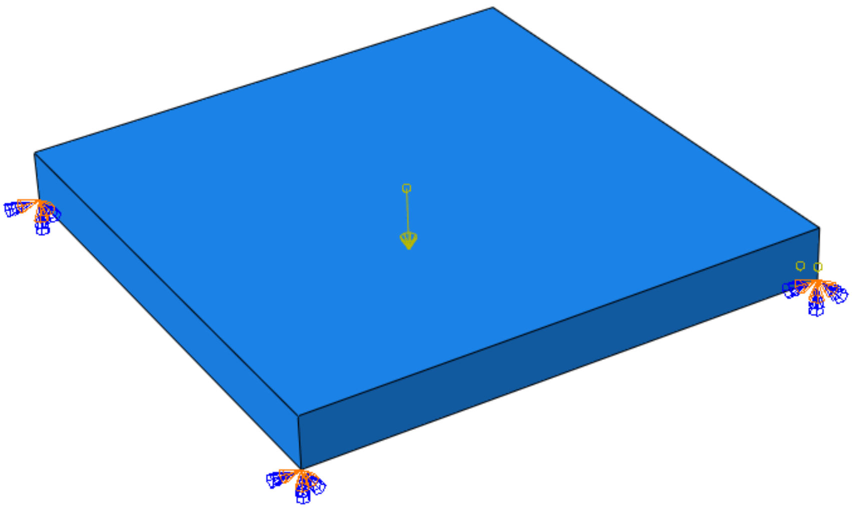

Figure 5: Boundary conditions imposed on slab models.

3.3. Four-Point Bending Test

The accuracy and reliability of the proposed numerical models were verified by conducting four-point flexural strength tests on selected HyFRC mix-design. Figure 6 shows the test setup for the experiment. Subsequently, only HyFRC 1, HyFRC 2, and HyFRC 5 were selected for verification along with the control RC slab specimen because of the encouraging results in the numerical analyses. HyFRC 1 was chosen because the performance improvement is very significant to the control specimen (122.02% in ultimate load, 88.36% in steel strain). Additionally, the performance of HyFRC 1, 3, 4, and 5 is marginally close, as seen in Figure 7. Hence, only HyFRC 2 and HyFRC 5 were chosen for experimental verification to observe the efficacy of the micro-macro combinations. The experiment had been previously simulated in ABAQUS software by implementing the constitutive models obtained from the uniaxial tests. Henceforth, the HyFRC slab specimens are identical to the models developed in FE analyses.

(a) LVDT locations

(b) Four-point flexural experimental test

(c) Slab molding with embedded rebars

(d) Casting of HyFRC slabs

Figure 6: Experimental setup and preparation.

4. Results and Discussion

4.1 Stress-Strain Behavior

Based on the compressive stress-strain curves shown in Figure 7(a), HyFRC 5 exhibited the highest improvement in the elastic region by 4.2%, followed by HyFRC 1 by 2.1%. It was observed that HyFRC 2, HyFRC 3, and HyFRC 4 slightly weakened the peak stress by 4.6%, 4.4%, and 5.0%. In the plastic region, significant improvement in the strain-softening curve was observed for HyFRC 2, HyFRC 4, and HyFRC 5, which effectively altered the failure mode of those concrete from brittle to quasi-brittle. However, the post-cracking behavior for HyFRC 1 and HyFRC 3 deteriorates more than the plain control specimen.

For HyFRC 1, the hybridization consists of only macro-sized fibers (38 and 54mm PP fibers). The diametrical size restricts the crack-bridging phenomenon to macro-cracks only, resulting in a weaker performance in the elastic stage due to the unbridged microcracks. However, the performance of HyFRC 1 in the plastic stage further deteriorated as the cracking widened into the post-cracking zone, primarily due to the localized dispersion of the fibers in the cement matrix. The fibers bridging phenomenon can only exist if the crack propagates perpendicular to the fibers, and the possibility increases if the fibers are widely dispersed in the cement matrix as opposed to a localized area.

For HyFRC 3, using P2 microfiber resulted in a fiber-breakage failure instead of debonding and pulling out. This process consumes less energy and negatively affects the concrete post-cracking resistance. The addition of P2 fibers provided the hybrid concrete with additional reinforcement through micro-crack bridging, which increases the peak stress of the concrete – creating stronger but brittle concrete [39]. After the hybrid concrete reached its peak stress, the rapid crack widening due to the brittle nature of the concrete resulted in the PP macrofibers breaking due to the applied forces being greater than the tensile strength of the fiber itself during fracture.

The tensile stress-strain curves are shown in Figure 7(b). In the elastic region, HyFRC 1 significantly increased the peak stress of control specimens, followed by HyFRC 3, HyFRC 2, HyFRC 5, and HyFRC 4. The fiber combinations improved the tensile peak stress by 32.8%, 30.7%, 18.3%, 15.8%, and 7.5%, respectively. Control specimens without fibers demonstrated instantaneous brittle failure during testing, while all the HyFRC specimens provided a significant strain-softening resistance in the plastic region indicating a quasi-brittle failure mode.

It can be observed that the mode of failure of concrete in both compression and tension changed from brittle to quasi-brittle with a strain-softening deterioration in the post-cracking region. The change is because of the fiber-bridging phenomenon by the macro-sized PP fibers inside the cement composite, which bridges widening cracks and delays the brittle fracture of the composite [40], [41].

In the compressive behavior, the developed HyFRC 2, HyFRC 3, and HyFRC 4 slightly deteriorated the compressive strength of plain control specimen. Several past studies have also shown that adding polypropylene fibers have reduced the compressive strength of concrete [42], [43]. The addition of P1, P2, and P3 fibers into the developed HyFRC deteriorated the compressive strength in the elastic region because of the fiber's low bond strength [44], and the breakage of Calcium Silicate Hydrate (C-S-H) bond between the cement and the aggregates [45].

This is because of the nature of cellulosic nylon materials, which is hydrophilic. Unlike polypropylene and polyethylene materials which are hydrophobic, nylon material absorbs water during concrete mixing. Excess water would gradually exude from the nylon and reacts with cement for further hydration [46]. This will cause additional strengthening of cement surrounding the nylon fibers and indirectly improve the interfacial bonding power of N fibers.

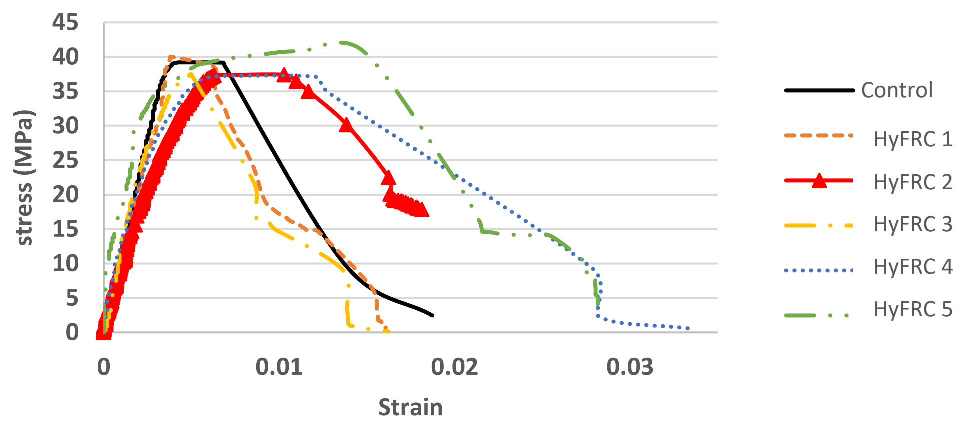

(a) Compressive behavior

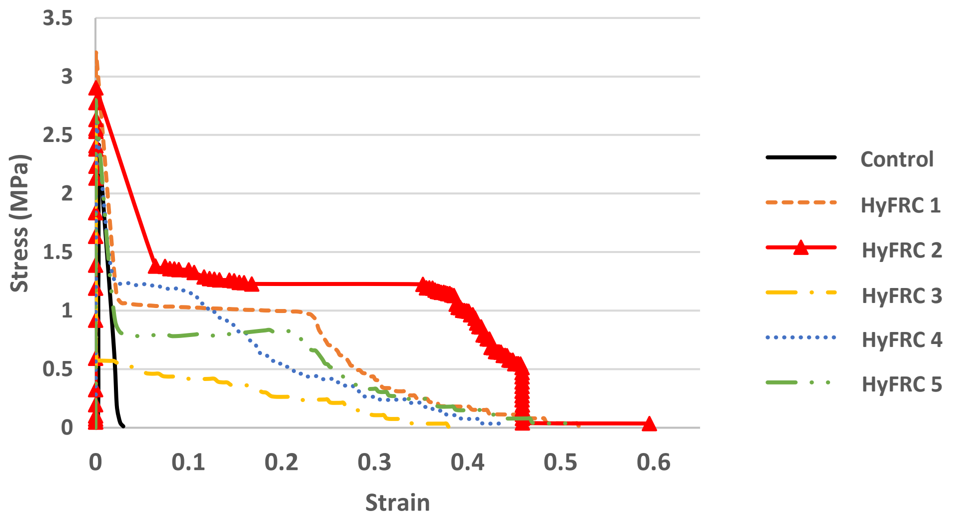

(b) Tensile behavior

Figure 7: Uniaxial tests for the developed HyFRC.

Table 4: Peak stress in compression and tension.

Mix Design	C	HyFRC 1	HyFRC 2	HyFRC 3	HyFRC 4	HyFRC 5
Compressive Strength (MPa)	39.20	40.03	37.41	37.48	37.23	40.85
Tensile Strength (MPa)	2.41	3.20	2.85	3.15	2.59	2.79

The peak stress in both compression and tension are shown in Table 4, it was observed that the absence of micro-class fibers in HyFRC 1 resulted in no significant improvement to the peak strength in compressive strength (2.10% difference) compared to plain control specimen. For HyFRC 5, the hydrophilic absorption of free water during concrete casting contributes more moisture for cement hydration. As a result, the cement area encircling the fibers is strengthened with additional C-S-H. Hence, N fibers are anchored securely in the cement matrix due to the improved interfacial bond [46]. The high tensile strength of N fibers and a strong interfacial

bond zone ensured that the fibers could gradually pull out without breakage and dissipate more energy, providing additional support to the RC slab during failure.
For the tensile behavior, the improved performance of the combined fibers in both the elastic and plastic regions is because of the utilization of micro and macro-sized fibers. Fibers can only bridge one level of crack depending on their fiber diameter [47]. The formation of small microcracks in the elastic region of cement composites is constrained by the micro-sized P1, P2, P3, and N fibers. These bridging of cracks evoke a multitracking phenomenon that prevents micro cracks from connecting unilaterally and propagating into a singular, larger macro crack [48], [49]. Similar studies have been observed concerning the enhanced post-cracking performance for HyFRC 2, HyFRC 3, HyFRC 4, and HyFRC 5, which have been embedded with both macro and microfibers as opposed to macrofibers-only HyFRC 1 [50], [51].

4.2 Numerical Analyses

Subsequently, the HyFRC stress-strain data from the uniaxial tests are used to define the damage in compression and tension during numerical modeling. The load-deflection curves for all HyFRC slabs and control specimens are shown in Figure 8. It can be deduced that adding fibers improved the RC slab's flexural performance by reducing deflection and resisting higher loads. A significant increase in the ultimate load capacity can be observed for HyFRC 2, with a 122.02% improvement from the control slab. This is followed by HyFRC 1, HyFRC 5, HyFRC 3, and HyFRC 4 with 54.42%, 38.67%, 21.24%, and 9.85% improvement, respectively. In brief, HyFRC 2 (strongest) > HyFRC 1 > HyFRC 5 > HyFRC 3 > HyFRC 4 (weakest).

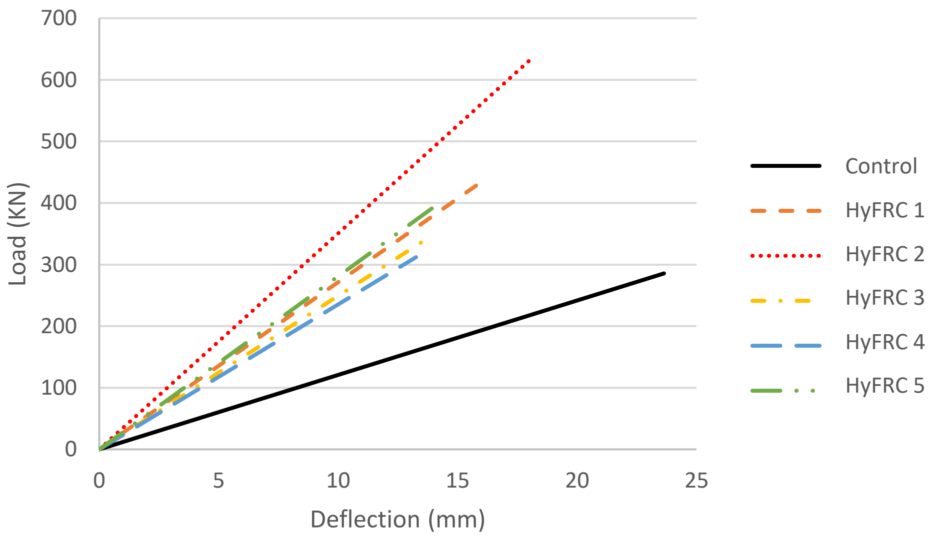

Figure 8: Load vs. deflection curves for HyFRC slabs.

However, the mid-span deflection is inversely proportional to the results obtained in the ultimate load capacity. HyFRC 4 resulted in the least improvement in ultimate load capacity yet reduced excessive deflection of the RC slabs the most by 42.34%. This is followed by HyFRC 3, HyFRC 5, HyFRC 1, and HyFRC 2 with a 39.94%, 39.37%, 37.97%, and 21.61% reduction in mid-span deflection. In descending order, HyFRC 4 (most stiff) > HyFRC 3 > HyFRC 5 > HyFRC 1 > HyFRC 2 (least stiff). The result for ultimate load capacity and mid-span deflection are shown in Table 5.

Table 5: Results for the load vs. deflection curves compared to the control slab model.

Specimen	Ultimate load Pmax (kN)	Difference (%)	Mid-span deflection (mm)	Difference (%)	Ultimate strain in steel (εs %)	Difference (%)
C	283.33	-	22.91	-	1.46	-
HyFRC 1	437.51	54.42	14.21	37.97	0.42	71.23
HyFRC 2	629.04	122.02	17.96	21.61	0.17	88.36
HyFRC 3	343.51	21.24	13.76	39.94	0.89	39.04
HyFRC 4	311.24	9.85	13.21	42.34	0.92	36.99
HyFRC 5	392.89	38.67	13.89	39.37	0.77	47.26

The fiber combinations in this study succeeded in reducing excessive strain imposed on the RC slab steel reinforcements. HyFRC 2 reduces 88.36% of the strain imposed on the steel reinforcements compared to the control slab, followed by HyFRC 1 (71.23%), HyFRC 5 (47.26%), HyFRC 3 (39.04%) and HyFRC 4 (36.99%). In sequential order, HyFRC 2 (highest) > HyFRC 1 > HyFRC 5 > HyFRC 3 > HyFRC 4 (lowest).

In addition, only linear data were analyzed as the CDP data obtained from the HyFRC constitutive models were not stable for detailed numerical analysis in the post-cracking stage (non-linear data) in Abaqus. Therefore, detailed tests were needed to obtain a precise constitutive response of all the HyFRC materials. However, this would be cost-ineffective and requires advanced testing to obtain unproven data to benefit cement composites significantly. Hence, only fundamental uniaxial stress-strain data were observed to evaluate the initial performance as well as for model verification. Based on these results, improvement can then be recommended before conducting more precise but costly constitutive tests for numerical analyses.

4.3 Experimental Validation

An experimental four-point bending test shown in Figure 11 was conducted to verify the results for the control (no fibers), HyFRC 1 (macro fibers only), and HyFRC 2 as well as HyFRC 5 (macro-micro fibers combined). HyFRC 2 was selected among the macro-micro fibers mix-design because it resulted in the best performance during the numerical analyses, while HyFRC 5 was tested to observe the efficacy of RC slabs with different hybrid fibers composition. The comparison between the experimental and numerical results is presented in Figure 10.

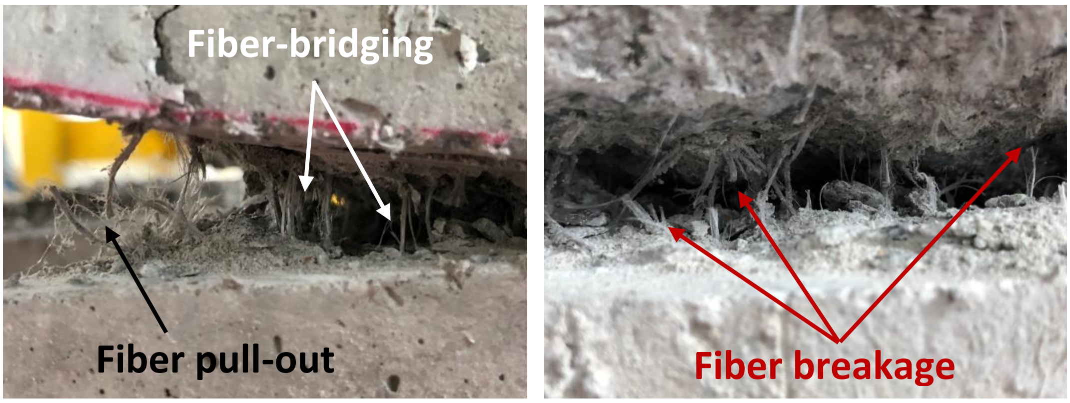

(a) Fiber bridging and pull-out (b) Fiber breakage

Figure 9: Focused view of fiber in the RC slab's crack propagation line.

The experimental and numerical data accuracies for the HyFRC slabs are below 20% for all assessed criteria, while the control specimens resulted in a slightly higher accuracy with an average of 13.92%. The percentage differences are tabulated in Table 6. It can be observed that the HyFRC slab improvement is expressly governed by the mode of failure of the fibers inside the concrete matrix. The fiber crack-bridging effect resists the propagation of flexural and shear cracks, as shown in Figure 12, which increases the ultimate load capacity of the HyFRC slabs. However, as the applied load exceeds the tensile limit of the fibers, the embedded fibers either fail in breakage or pull out. The transfer of load between the fibers and the concrete matrix during fiber breakage and pull-out determines the extent of improvement of the RC slab in post-cracking behavior. HyFRC slabs experiencing fiber breakage would result in less improvement than HyFRC slabs undergoing fiber pull-out failure as the energy dissipated during the pull-out friction significantly improves the post-cracking ability of the matrix host [39], [52]. A focused view of the crack propagation line on the RC slab is shown in Figure 9, showing the various fiber failure modes during the experimental tests.

Table 6: Comparison between numerical and experimental results.

Slab	**Verification**	**Ultimate load P_{max} (kN)**	**Mid-span deflection (mm)**	**Ultimate strain in steel εs %**	**Percentage Difference, %**		
					P_{max}	**Deflection**	**εs**
C	Experimental	243.01	19.01	1.35	15.32	18.61	7.83
	Numerical	283.33	22.91	1.46			
HyFRC 1	Experimental	350.15	12.06	0.35	22.18	16.37	18.18
	Numerical	437.51	14.21	0.42			
HyFRC 2	Experimental	512.12	16.21	0.14	20.48	10.16	19.35
	Numerical	629.04	17.96	0.17			
HyFRC 5	Experimental	370.56	11.39	0.44	14.27	19.78	16.67
	Numerical	392.89	13.89	0.52			

Accordingly, the decrease in strain is because of the additional resistance provided by the fibers in resisting excessive loads transferred to the steel reinforcements through the concrete matrix. The result is consistent with past research on synthetic fibers and their effect on steel reinforcements [53].

4.4 Cracking Pattern

In the numerical analyses, the cracking patterns on the tension surface of the HyFRC slabs were similar. For HyFRC slabs, the first crack on the tension face occurred at loads higher than the service load. The cracking loads were 45, 55, 41, 39, and 44 KN for slabs HyFRC 1, HyFRC 2, HyFRC 3, HyFRC 4, and HyFRC 5, respectively. For the control slab, C, the first cracks appeared directly under the loaded area under the center of the slabs. Then, additional cracks started to appear away from the loaded area at the center of the slabs. Finally, before failure, a roughly circular crack appeared and propagated to form the punching shear circle at the bottom face of the slabs. The comparisons between experimental cracking patterns and FE models are shown in Figure 14.

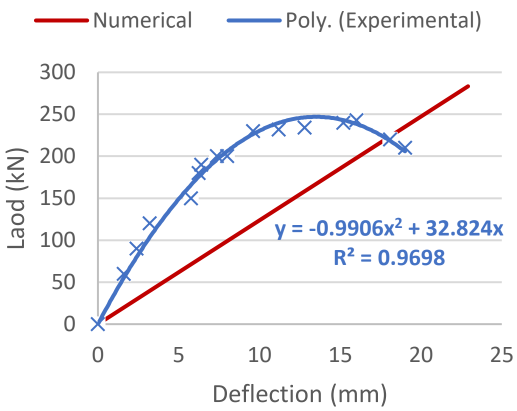

(a) Control slab

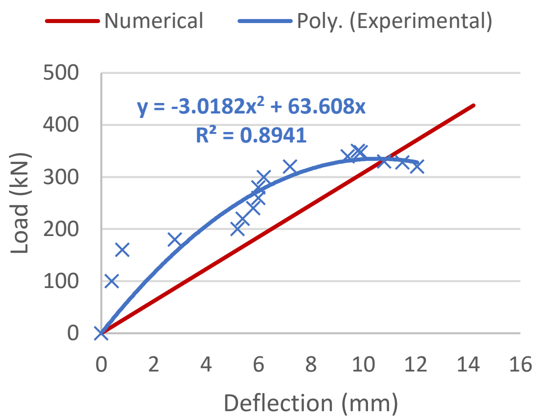

(b) HyFRC 1 slab

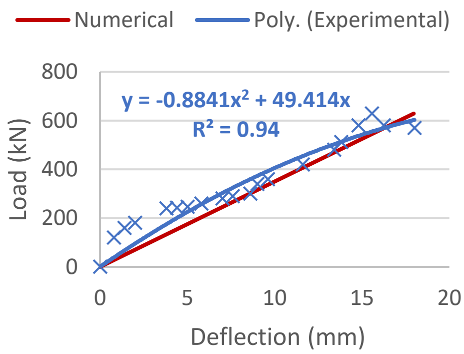

(c) HyFRC 2 slab

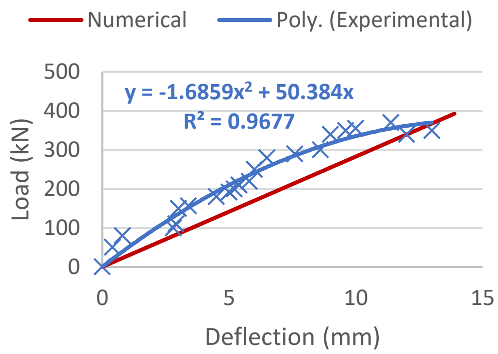

(d) HyFRC 5 slab

Figure 10: Load vs. Deflection curves for experimental and numerical results.

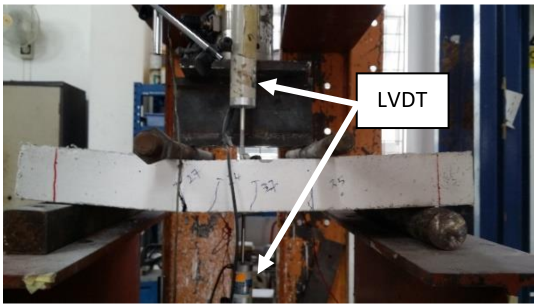

(a) Control Slab

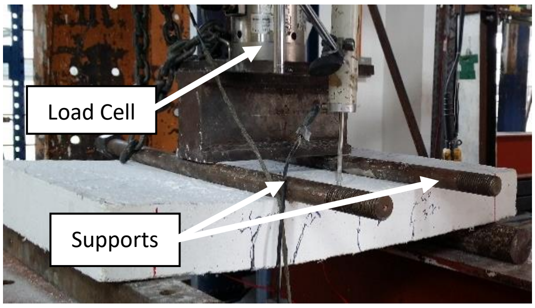

(b) HyFRC Slab

Figure 11: Deflection of slabs during the four-point bending test

(a) Crack-bridging of fibers

(b) Crack propagation under slabs

Figure 12: Fiber mode of failure and crack pattern of slabs specimens

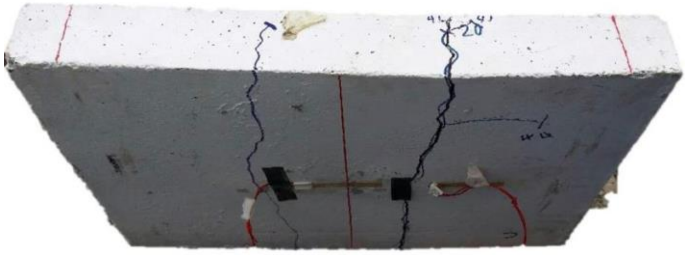

(a) Control slab

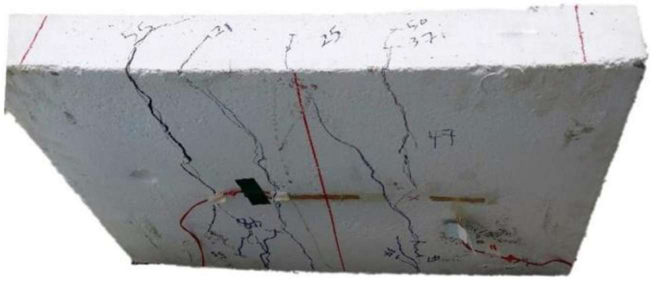

(b) HyFRC 1 slab

(c) HyFRC 2 slab

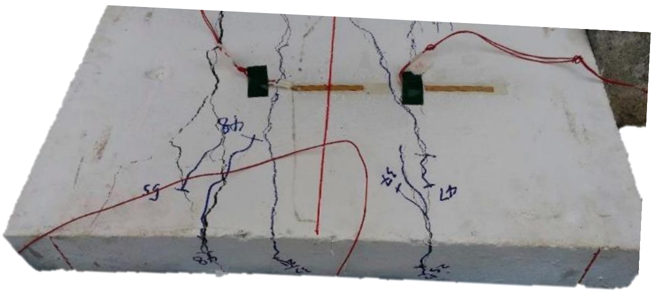

(d) HyFRC 5 slab

Figure 13: Slab specimens cracking pattern

For the HyFRC slabs, the first crack on the top face occurred at a high load. The first cracks appeared directly above the support and were oriented in the longitudinal direction parallel to the support, then moved in a circular direction to form incomplete circles. This indicates that the type of reinforcement had no significant influence on the cracking behavior of the tested slabs. It can also be observed that the control slab has a more uniform and singular crack propagation than HyFRC 1, HyFRC 2, and HyFRC 5. Contrastingly, the addition of fibers enabled a multicracking phenomenon in the concrete, improving the RC slab's flexural strength as a whole. The fiber bridging effect of fibers prevented singular propagation of cracks from micro to macro scale and evoke new crack propagation pathways. This dissipates more energy and improves the toughness of the slab. The final crack patterns of the experimentally tested slabs are shown in Figure 13.

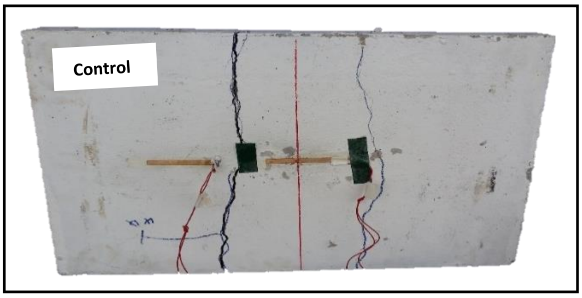

(a) Control RC Slab

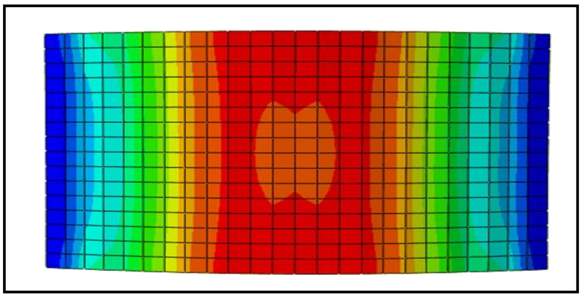

(b) Control numerical mode

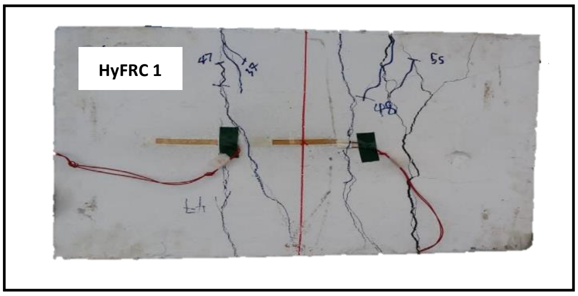

(c) HyFRC 1 RC Slab

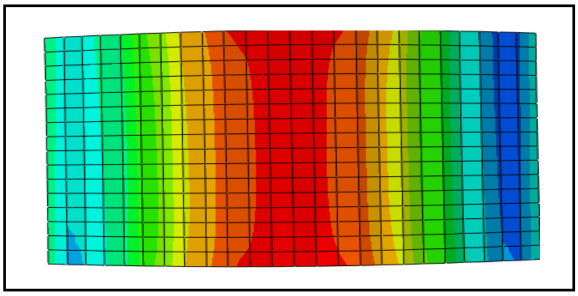

(d) HyFRC 1 numerical model

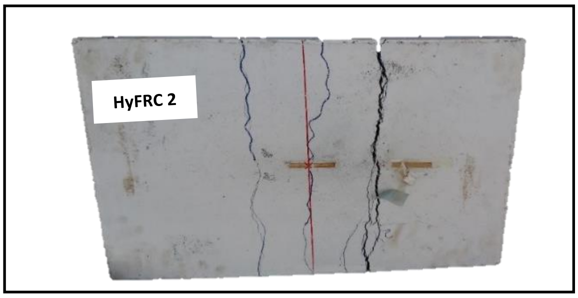

(e) HyFRC 2 RC Slab

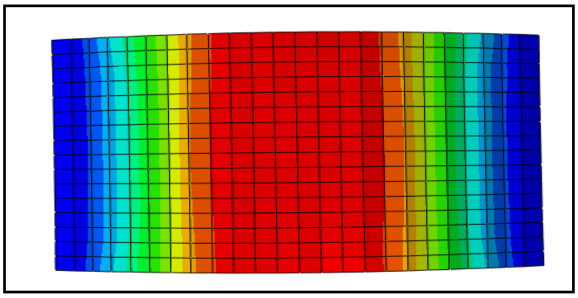

f) HyFRC 2 numerical model

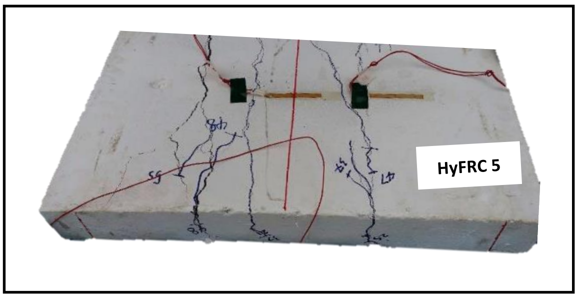

(e) HyFRC 5 RC Slab

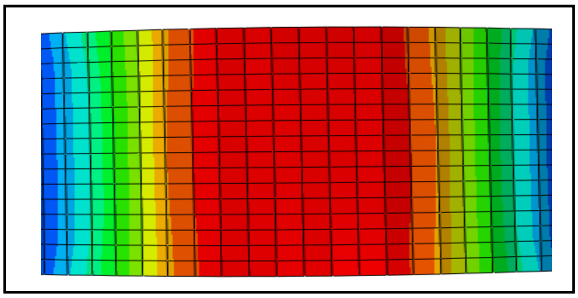

f) HyFRC 5 numerical model

Figure 14: Experimental vs. numerical cracking patterns.

5. Conclusion

An attempt has been made to improve the performance of RC slabs under a four-point bending test by incorporating hybrid synthetic fibers inside the concrete mix. Finite Element models were developed from this new material and subsequently validated through experimental testing. The conclusions drawn from this study and analyses are as follows:

- The inclusion of hybrid synthetic fibers has improved the tensile and compressive behavior of plain cement composite. However, certain synthetic fibers combination (HyFRC 2, HyFRC 3, HyFRC 4) deteriorated the compressive performance in the elastic stage.
- Significant improvements were observed in HyFRC slabs regarding the ultimate load capacity, corresponding mid-span deflection, steel reinforcement strain output, and cracking behavior compared to conventional RC slabs.
- A good agreement has been established between the HyFRC experimental and numerical slab results, with an average accuracy of 18.98% for the ultimate load capacity, 15.44% for the mid-span deflection, and 18.21% for steel strain output.

Acknowledgment

The authors would like to express appreciation to Innofloor Sdn. Bhd. for providing the fibers in this study, as well as appreciation to Universiti Malaysia Sabah for providing the SPLB research grant to conduct this research (Code: SLB 2107)

References

[1] J. Thomas and A. Ramaswamy, “Mechanical Properties of Steel Fiber-Reinforced Concrete,” *J. Mater. Civ. Eng. @ ASCE*, vol. 19, no. May, pp. 385–392, 2007, doi: 10.1061/ASCE0899-1561200719:5385.

[2] J. R. Roesler, S. A. Altoubat, D. A. Lange, K. A. Rieder, and G. R. Ulreich, “Effect of synthetic fibers on structural behavior of concrete slabs-on-ground,” *ACI Mater. J.*, vol. 103, no. 1, pp. 3–10, 2006.

[3] N. Buratti, C. Mazzotti, and M. Savoia, “Post-cracking behaviour of steel and macro-synthetic fibre-reinforced concretes,” *Constr. Build. Mater.*, vol. 25, no. 5, pp. 2713–2722, 2011, doi: 10.1016/j.conbuildmat.2010.12.022.

[4] A. Khanlou, G. MacRae, A. Scott, S. Hicks, and G. Clifton, “Shear performance of steel fibre-reinforced concrete,” in *Australasian Structural Engineering Conference*, 2012, vol. 1, no. 2006, p. 8. doi: 10.1111/joa.12446.

[5] A. E. Naaman, “Engineered Steel Fibers with Optimal Properties for Reinforcement of Cement Composites,” *J. Adv. Concr. Technol.*, vol. 1, no. 3, pp. 241–252, 2007, doi: 10.3151/jact.1.241.

[6] A. C1116/C1116M-15, “Standard Specification for Fiber-Reinforced Concrete,” *ASTM Int.*, no. Reapproved 2015, pp. 1–7, 2014, doi: 10.1520/C1116.

[7] Z. Zheng and D. Feldman, “Synthetic Fibre-Reinforced Concrete,” *Prog. Polym. Sci.*, vol. 20, no. 94, pp. 185–210, 1995.

[8] F. Salvador Cesa, A. Turra, and J. Baruque-Ramos, “Synthetic fibers as microplastics in the marine environment: A review from textile perspective with a focus on domestic washings,” *Sci. Total Environ.*, vol. 598, pp. 1116–1129, 2017, doi: 10.1016/j.scitotenv.2017.04.172.

[9] S. C. McCraven, “Fibers for Tomorrow,” *Concrete Construction*, pp. 27–30, 2002.

[10] A. M. Alani and D. Beckett, “Mechanical properties of a large scale synthetic fibre reinforced concrete ground slab,” *Constr. Build. Mater.*, vol. 41, pp. 335–344, 2013, doi: 10.1016/j.conbuildmat.2012.11.043.

[11] C. Röhm, B. Novák, S. Sasmal, R. Karusala, and V. Srinivas, “Behaviour of fibre reinforced beam-column sub-assemblages under reversed cyclic loading,” *Constr. Build. Mater.*, vol. 36, pp. 319–329, 2012, doi: 10.1016/j.conbuildmat.2012.04.114.

[12] A. A. Abbas, S. M. Syed Mohsin, and D. M. Cotsovos, “Seismic response of steel fibre reinforced concrete beam-column joints,” *Eng. Struct.*, vol. 59, pp. 261–283,

2014, doi: 10.1016/j.engstruct.2013.10.046.
[13] R. M. Oinam, D. R. Sahoo, and R. Sindhu, "Cyclic response of Non-ductile rc frame with steel fibers at Beam-Column joints and plastic hinge regions," *J. Earthq. Eng.*, vol. 18, no. 6, pp. 908–928, 2014, doi: 10.1080/13632469.2014.916239.
[14] R. Zhang, K. Matsumoto, T. Hirata, Y. Ishizeki, and J. Niwa, "Application of PP-ECC in beam-column joint connections of rigid-framed railway bridges to reduce transverse reinforcements," *Eng. Struct.*, vol. 86, pp. 146–156, 2015, doi: 10.1016/j.engstruct.2015.01.005.
[15] Q. Fu, D. Niu, J. Zhang, D. Huang, and M. Hong, "Impact response of concrete reinforced with hybrid basalt-polypropylene fibers," *Powder Technol.*, vol. 326, pp. 411–424, 2018, doi: 10.1016/j.powtec.2017.12.022.
[16] W. Yao *et al.*, "Influence of fiber mixture on impact response of ultra-high-performance hybrid fiber reinforced cementitious composite," *Compos. Part B Eng.*, vol. 163, no. May 2018, pp. 487–496, 2019, doi: 10.1016/j.compositesb.2018.12.141.
[17] Y. Swolfs, L. Gorbatikh, and I. Verpoest, "Fibre hybridization in polymer composites: A review," *Compos. Part A Appl. Sci. Manuf.*, vol. 67, pp. 181–200, 2014, doi: 10.1016/j.compositesa.2014.08.027.
[18] S. Guler, "The effect of polyamide fibers on the strength and toughness properties of structural lightweight aggregate concrete," *Constr. Build. Mater.*, vol. 173, pp. 394–402, 2018, doi: 10.1016/j.conbuildmat.2018.03.212.
[19] R. Siva Chidambaram and P. Agarwal, "Performance Evaluation of Metallic and Synthetic Fiber Hybridization on the Cyclic Behavior of Exterior Beam-Column Joint," *Adv. Civ. Eng. Mater.*, vol. 7, no. 1, p. 20170137, 2018, doi: 10.1520/acem20170137.
[20] S. K. Nayar and R. Gettu, "Synergy in toughness by incorporating amorphous metal and steel fibers," *ACI Mater. J.*, vol. 112, no. 6, pp. 821–827, 2015, doi: 10.14359/51687857.
[21] S. P. Yap, C. H. Bu, U. J. Alengaram, K. H. Mo, and M. Z. Jumaat, "Flexural toughness characteristics of steel-polypropylene hybrid fibre-reinforced oil palm shell concrete," *Mater. Des.*, vol. 57, pp. 652–659, 2014, doi: 10.1016/j.matdes.2014.01.004.
[22] D. R. Sahoo, A. Solanki, and A. Kumar, "Influence of Steel and Polypropylene Fibers on Flexural Behavior of RC Beams," *J. Mater. Civ. Eng.*, vol. 27, no. 8, p. 04014232, 2014, doi: 10.1061/(asce)mt.1943-5533.0001193.
[23] M. N. Soutsos, T. T. Le, and A. P. Lampropoulos, "Flexural performance of fibre reinforced concrete made with steel and synthetic fibres," *Constr. Build. Mater.*, vol. 36, pp. 704–710, 2012, doi: 10.1016/j.conbuildmat.2012.06.042.
[24] K. H. Mo, S. H. Goh, U. J. Alengaram, P. Visintin, and M. Z. Jumaat, "Mechanical, toughness, bond and durability-related properties of lightweight concrete reinforced with steel fibres," *Mater. Struct. Constr.*, vol. 50, no. 1, 2017, doi: 10.1617/s11527-016-0934-1.
[25] F. Zhang, Y. Ding, J. Xu, Y. Zhang, W. Zhu, and Y. Shi, "Shear strength prediction for steel fiber reinforced concrete beams without stirrups," *Eng. Struct.*, vol. 127, pp. 101–116, 2016, doi: 10.1016/j.engstruct.2016.08.012.
[26] K. Wille and A. E. Naaman, "Pull-out behavior of high-strength steel fibers embedded in ultra-high-performance concrete," *ACI Mater. J.*, vol. 109, no. 4, pp. 479–488, 2012.
[27] S. Yin, R. Tuladhar, T. Collister, M. Combe, and N. Sivakugan, "Mechanical Properties and Post-crack Behaviours of Recycled PP Fibre Reinforced Concrete," in *Concrete 2015*, 2015, no. August.

[28] L. Strezov and J. Herbertson, “A Life Cycle Perspective on Steel Building Materials,” 2006. Accessed: Feb. 26, 2019. [Online]. Available: https://www.yumpu.com/en/document/read/31684244/a-life-cycle-perspective-on-steel-building-materials-onesteel

[29] L. Shen, E. Worrell, and M. K. Patel, “Open-loop recycling: A LCA case study of PET bottle-to-fibre recycling,” *Resour. Conserv. Recycl.*, vol. 55, no. 1, pp. 34–52, 2010, doi: 10.1016/j.resconrec.2010.06.014.

[30] R. S. Chidambaram and P. Agarwal, “Seismic behavior of hybrid fiber reinforced cementitious composite beam-column joints,” *Mater. Des.*, vol. 86, pp. 771–781, 2015, doi: 10.1016/j.matdes.2015.07.164.

[31] N. Banthia and N. Nandakumar, “Crack Growth Resistance of Hybrid Fiber Reinforced Cement Composites,” *Cem. Concr. Compos.*, vol. 25, no. 1, pp. 3–9, 2003.

[32] H. R. Pakravan and T. Ozbakkaloglu, “Synthetic fibers for cementitious composites: A critical and in-depth review of recent advances,” *Constr. Build. Mater.*, vol. 207, pp. 491–518, 2019, doi: 10.1016/j.conbuildmat.2019.02.078.

[33] P. K. Nelson, V. C. Li, and T. Kamada, “Fracture Toughness of Microfiber Reinforced Cement Composites,” *J. Mater. Civ. Eng.*, vol. 14, no. 5, pp. 384–391, 2002, doi: 10.1061/(ASCE)0899-1561(2002)14:5(384).

[34] ASTM C150-07, “Standard Specification for Portland Cement.” ASTM International, 2007.

[35] ASTM C494/C494M-17, “Standard Specification for Chemical Admixtures for Concrete,” *ASTM International*. 2017. doi: 10.1520/C0494.

[36] ASTM 469/C469M-14, “Standard Test Method for Static Modulus of Elasticity and Poisson’s Ratio of Concrete,” *ASTM International*. 2014. doi: 10.1520/C0469.

[37] A. M. T. Hassan, S. W. Jones, and G. H. Mahmud, “Experimental test methods to determine the uniaxial tensile and compressive behaviour of Ultra High Performance Fibre Reinforced Concrete(UHPFRC),” *Constr. Build. Mater.*, vol. 37, pp. 874–882, 2012, doi: 10.1016/j.conbuildmat.2012.04.030.

[38] E8/E8M-16a, “Standard Test methods for Tension Testing of Metallic Materials,” *ASTM International*. 2010. doi: 10.1520/E0008.

[39] J. Lawler, D. Zampini, and S. Shah, “Microfiber and Macrofiber Hybrid Fiber-Reinforced Concrete,” *J. Mater. Civ. Eng.*, vol. 17, no. 5, pp. 595–604, 2005, doi: 10.1061/(ASCE)0899-1561(2005)17:5(595).

[40] K. Yu, Y. Wang, J. Yu, and S. Xu, “A strain-hardening cementitious composites with the tensile capacity up to 8%,” *Constr. Build. Mater.*, vol. 137, pp. 410–419, 2017, doi: 10.1016/j.conbuildmat.2017.01.060.

[41] F. S. Khalid, J. M. Irwan, M. H. Wan Ibrahim, N. Othman, and S. Shahidan, “Splitting tensile and pull-out behavior of synthetic wastes as fiber-reinforced concrete,” *Constr. Build. Mater.*, vol. 171, pp. 54–64, 2018, doi: 10.1016/j.conbuildmat.2018.03.122.

[42] H. Aljewifi, “Influence of Polypropylene Fibers on Mechanical Properties of Different Concrete Mixtures,” *Int. J. Adv. Eng. Technol.*, vol. 9, no. 5, pp. 513–522, 2016.

[43] A. Sadrmomtazi and A. K. Haghi, “Properties of cementitious composites containing polypropylene fiber waste,” *Compos. Interfaces*, vol. 15, no. 7–9, pp. 867–879, 2008, doi: 10.1163/156855408786778294.

[44] Alan E. Richardson, “Bond characteristics of structural polypropylene fibres in concrete with regard to post-crack strength and durable design,” *Struct. Surv.*, vol. 23, no. 3, pp. 210–230, 2005.

[45] Alan E. Richardson, “Compressive strength of concrete with polypropylene fibre additions,” *Struct. Surv.*, vol. 24, no. 1, pp. 138–153, 2006.

[46] A. Bentur and S. Akers, “The microstructures and ageing of cellulose fiber reinforced

cement composites cured in a normal environment," *Int. J. Cem. Compos. Light. Concr.*, vol. 11, no. 2, pp. 99–109, 1989.

[47] L. R. Betterman, C. Ouyang, and S. P. Shah, "Fiber-matrix interaction in microfiber-reinforced mortar," *Adv. Cem. Based Mater.*, vol. 2, no. 2, pp. 53–61, 1995, doi: 10.1016/1065-7355(95)90025-X.

[48] D. Y. Yoo and M. J. Kim, "High energy absorbent ultra-high-performance concrete with hybrid steel and polyethylene fibers," *Constr. Build. Mater.*, vol. 209, pp. 354–363, 2019, doi: 10.1016/j.conbuildmat.2019.03.096.

[49] M. J. Kim, D. Y. Yoo, and Y. S. Yoon, "Effects of geometry and hybrid ratio of steel and polyethylene fibers on the mechanical performance of ultra-high-performance fiber-reinforced cementitious composites," *J. Mater. Res. Technol.*, vol. 8, no. 2, pp. 1835–1848, 2019, doi: 10.1016/j.jmrt.2019.01.001.

[50] N. Banthia, F. Majdzadeh, J. Wu, and V. Bindiganavile, "Fiber synergy in Hybrid Fiber Reinforced Concrete (HyFRC) in flexure and direct shear," *Cem. Concr. Compos.*, vol. 48, pp. 91–97, 2014, doi: 10.1016/j.cemconcomp.2013.10.018.

[51] S. G. Chasioti and F. J. Vecchio, "Effect of fiber hybridization on basic mechanical properties of concrete," *ACI Struct. J.*, vol. 114, no. 3, pp. 375–384, 2017, doi: 10.14359/51689479.

[52] N. Banthia and J. Sheng, "Micro-reinforced Cementitious Materials," *MRS Proc.*, vol. 211, pp. 25–32, 1991.

[53] D. Kheni, R. H. Scott, S. K. Deb, and A. Dutta, "Ductility enhancement in beam-column connections using hybrid fiber-reinforced concrete," *ACI Struct. J.*, vol. 112, no. 2, pp. 167–178, 2015, doi: 10.14359/51687405.